ELSEVIER

NeuroImage

www.elsevier.com/locate/ynimg
NeuroImage 41 (2008) 277–285

Structural and functional biomarkers of prodromal Alzheimer's disease: A high-dimensional pattern classification study

Yong Fan,[a] Susan M. Resnick,[b] Xiaoying Wu,[a] and Christos Davatzikos[a,*]

[a]*Section of Biomedical Image Analysis, Department of Radiology, University of Pennsylvania, PA, USA*
[b]*Laboratory of Personality and Cognition, National Institute on Aging, MD, USA*

Received 18 October 2007; revised 12 February 2008; accepted 20 February 2008
Available online 6 March 2008

This work builds upon previous studies that reported high sensitivity and specificity in classifying individuals with mild cognitive impairment (MCI), which is often a prodromal phase of Alzheimer's disease (AD), via pattern classification of MRI scans. The current study integrates MRI and PET ^{15}O water scans from 30 participants in the Baltimore Longitudinal Study of Aging, and tests the hypothesis that joint evaluation of structure and function can yield higher classification accuracy than either alone. Classification rates of up to 100% accuracy were achieved via leave-one-out cross-validation, whereas conservative estimates of generalization performance in new scans, evaluated via bagging cross-validation, yielded an area under the receiver operating characteristic (ROC) curve equal to 0.978 (97.8%), indicating excellent diagnostic accuracy. Spatial maps of regions determined to contribute the most to the classification implicated many temporal, prefrontal, orbitofrontal, and parietal regions. Detecting complex patterns of brain abnormality in early stages of cognitive impairment has pivotal importance for the detection and management of AD.

Keywords: Alzheimer's disease; MCI; High-dimensional pattern classification; MRI; PET; Voxel-based analysis; Diagnosis of AD

Amnestic mild cognitive impairment (MCI) is often a prodromal stage to Alzheimer's disease (AD), as individuals with MCI may convert to AD at an annual rate as high as 15% (Petersen et al., 1999). Therefore, MCI is frequently considered to be a good target for early AD diagnosis, and for therapeutic interventions. MRI and PET imaging can potentially be used as diagnostic tools that assess brain structure and function in a direct and objective way and have potential utility for diagnosis, prognosis, and evaluation of disease progression and treatment effects.

Many imaging studies have found loss of grey matter (GM) and metabolic abnormalities in MCI. Most of the earlier studies were based on volumetric measurements of regions of interest (ROIs) (Chetelat et al., 2002; Convit et al., 2000; Dickerson et al., 2001; Fox et al., 1996a; Kaye et al., 1997; Killiany et al., 2000), such as the hippocampus and the entorhinal cortex, and have confirmed GM atrophy in regions that are known to be affected by AD. However, the pattern of AD pathology is complex and evolves as the disease progresses, starting mainly in the hippocampus and entorhinal cortex, and subsequently spreading throughout temporal and orbitofrontal cortex, posterior cingulate, and association cortex generally (Braak et al., 1998). Therefore, measuring volumes or average PET signals of a few structures cannot capture the spatio-temporal pattern of structural and physiological abnormalities in their entirety. Moreover, measurements of hand-drawn ROIs are not easily reproducible within and across different raters. Last but not least, the pattern of disease progression does not necessarily follow pre-determined anatomical boundaries.

Voxel-based morphometry (VBM) has been proposed by a number of investigators as a more comprehensive way of measuring the spatial distribution of brain atrophy in MCI and AD, by evaluating images region by region instead of making *a priori* assumptions about specific ROIs. A variety of VBM-type methods exist (Ashburner and Friston, 2000; Chung et al., 2001; Davatzikos et al., 2001, 1996; Thompson et al., 2001), which generally fall under the umbrella of the field of computational neuroanatomy (Ashburner et al., 2003; Miller et al., 1997). VBM studies have confirmed that complex spatial patterns of brain atrophy can be measured in MCI and AD (Bozzali et al., 2006; Chetelat et al., 2002; Davatzikos et al., 2008; Karas et al., 2004; Pennanen et al., 2005a; Saykin et al., 2006; Thompson et al., 2001; Whitwell et al., 2007; Xie et al., 2006). However, VBM analyses are of limited value for individual diagnosis, since they measure group differences and are not equipped to classify individuals. Towards this goal, high-dimensional pattern classification methods have

* Corresponding author. Department of Radiology, University of Pennsylvania, 3600 Market Street, Suite 380, Philadelphia, PA 19104, USA. Fax: +1 215 614 0266.
E-mail address: christos@rad.upenn.edu (C. Davatzikos).
Available online on ScienceDirect (www.sciencedirect.com).

1053-8119/$ - see front matter © 2008 Elsevier Inc. All rights reserved.
doi:10.1016/j.neuroimage.2008.02.043

been pursued in recent years (Davatzikos, 2004; Duchesne et al., 2006; Fan et al., 2006a, 2007a, 2005, 2006b, 2007b; Golland et al., 2002; Lao et al., 2004; Liu et al., 2004; Timoner et al., 2002), and have shown great potential in a variety of neuroimaging studies (Davatzikos et al., 2008, 2005a,b; Fan et al., 2008a, 2005, 2006b, 2007b, Kawasaki et al., 2007; Mourao-Miranda et al., 2005; Yoon et al., 2007). Unlike VBM-type methods, which are mass univariate and don't consider statistical associations among different brain regions, high-dimensional pattern classification methods are multivariate, thereby leading to better group separation, which is critical for individual diagnosis. Put differently, no brain region has sufficient sensitivity and specificity in identifying individuals at risk for AD, or even with AD, due to high inter-individual variability. However combinations of measurements from many different regions and imaging modalities can potentially build patterns of high discriminative power.

The current study builds upon previous work in Davatzikos et al. (2008), aiming to construct an imaging-based diagnostic method for individuals with MCI, using data from a prospective longitudinal study of aging (Resnick et al., 2000). In our prior study, we were able to discriminate structural MRI scans of individuals with MCI from cognitively normal individuals with accuracy up to 90%, upon cross-validation. In the current paper, we investigate the added value of combining structural MRI and PET images of regional cerebral blood flow (rCBF) in discriminating between MCI and normal controls. We apply techniques of adaptive regional feature extraction, feature selection, and multivariable support vector machine classification, which construct a multivariable classifier by learning from training samples (Fan et al., 2005, 2007b). In addition, we extend our approach using a technique called bagging (Breiman, 1996; Duda et al., 2001; Fan et al., 2008b), to obtain more conservative estimates of how well this approach is likely to generalize to new individuals. This study is therefore the first to demonstrate the potential of pattern classification methods applied to a combination of structural MRI and functional PET images in achieving highly sensitive and specific diagnostic accuracy in MCI.

Methods

Participants

MRI scans from 30 elderly individuals were obtained annually as part of the Baltimore Longitudinal Study of Aging (BLSA) neuroimaging substudy (Resnick et al., 2000). The BLSA neuroimaging study, initiated in 1994, is a prospective study of brain structure and function in older adults, which investigates structural, functional, and cognitive changes associated with normal aging and cognitive impairment. At initial enrollment, all individuals were free of dementia and other central nervous system disorders, severe cardiovascular disease, and metastatic cancer (detailed in Resnick et al. (2000)). Screening of mental status by the Blessed-Information-Memory-Concentration (BIMC) test was performed at each annual visit in conjunction with a comprehensive neuropsychological assessment. Subject and informant-based assessments with the Clinical Dementia Rating (CDR) (Morris et al., 1989) scale were administered by certified examiners to participants in the BLSA autopsy study annually (about 50% of participants) and to the remaining participants scoring 3 or more BIMC errors. Individuals with 3 or more BIMC errors or a 0.5 CDR were reviewed at prospective diagnostic case conferences. A diagnosis of MCI was made for participants who had deficits in either a single cognitive domain (usually memory) or had more than one cognitive deficit but did not have functional loss in activities of daily living. MRI and PET images were not used during the case conferences, although MRI interpretative reports were available. From a sample of 158 neuroimaging study participants who completed as many as 9 annual neuroimaging and cognitive assessments, 15 participants were characterized as MCI and were matched for age, sex, and follow-up interval to 15 who remained unimpaired (CDR = 0). These individuals, who are identified within the context of prospective longitudinal follow-ups, typically represent relatively mild cases of cognitive impairment in contrast to those followed in other studies (e.g. Grundman et al. (2004)). Therefore, in this group AD pathology is likely to be at relatively early stages. The current study involved a cross-sectional analysis, using MRI and PET scans obtained at the most recent assessment or the assessment prior to dementia diagnosis for each MCI individual. Subject characteristics are shown in Table 1.

Imaging protocol

MR acquisition procedures are detailed in Resnick et al. (2000). MR scanning was performed on a GE Signa 1.5 T scanner. The current results are based on a high-resolution volumetric "spoiled grass" (SPGR) series (axial acquisition, TR = 35, TE = 5, flip angle = 45, FOV = 24, matrix = 256 × 256, NEX = 1, voxel dimensions of 0.94 × 0.94 × 1.5 mm slice thickness). Resting PET images of participants were acquired on a GE 4096+ scanner which provides 15 slices of 6.5 mm thickness. During scanning, participants were instructed to keep their eyes open and focused on a computer screen covered by a black cloth. PET measures of rCBF were obtained using [^{15}O] water. Images were acquired for 60 s from the time the total radioactivity counts in brain reached threshold level. A transmission scan acquired before the emission scans was used to perform attenuation correction.

Image analysis

Image pre-processing was performed according to the protocol that has been described and validated in Davatzikos et al. (2001) and Goldszal et al. (1998). The pre-processing steps included 1) alignment to the AC–PC plane; 2) removal of extra-cranial material (skull-stripping); 3) tissue segmentation into grey matter (GM), white matter (WM), and cerebrospinal fluid (CSF), using a brain tissue segmentation method proposed in Pham and Prince (1999); 4) high-dimensional image warping (Shen and Davatzikos, 2002) to a standardized coordinate system, a brain atlas (template) that was aligned with the MNI coordinate space (Kabani et al., 1998);

Table 1
Characteristics of the participants in this MCI study

Group	MCI	Normal
No. of subjects	15	15
Sex no. of males	10	10
No. of left-handed	0	1
Years of education, mean (SD)	15.8 (3.7)	16.7 (3.2)
Baseline age (year), mean (SD)	76.9 (7.3)	75.2 (6.8)
Age at last visit (year), mean (SD)	82.4 (6.6)	81.2 (6.4)
Follow-up interval (year), mean (SD)	5.5 (2.4)	6.6 (2.5)
Baseline MMSE, mean (SD)	27.5 (2.5)	28.2 (1.7)
MMSE at last visit, mean (SD)	25.8 (3.0)	29.0 (1.4)

and 5) formation of regional volumetric maps, named RAVENS maps (Davatzikos et al., 2001; Goldszal et al., 1998; Shen and Davatzikos, 2003), using tissue-preserving image warping (Goldszal et al., 1998). RAVENS maps quantify the regional distribution of GM, WM, and CSF; one RAVENS map is formed for each tissue type. In particular, if the image warping transformation that registers an individual scan with the template applies an expansion to a GM structure, the GM density of the structure decreases accordingly to insure that the total amount of GM is preserved. Conversely, a RAVENS value increases during contraction if tissue from a relatively larger region is compressed to fit a smaller region in the template. Consequently, RAVENS values in the template's (stereotaxic) space are directly proportional to the volume of the respective structures in the original brain scan. Therefore, regional volumetric measurements and comparisons are performed via measurements and comparisons of the respective RAVENS maps. For example, patterns of GM atrophy in the temporal lobe are quantified by patterns of RAVENS decrease in the temporal lobe in the stereotaxic space. In order to account for variations in head size, RAVENS maps were normalized by total intra-cranial volume (ICV).

The RAVENS approach has been extensively validated (Davatzikos et al., 2001; Goldszal et al., 1998) and applied to a variety of studies (Beresford et al., 2006a,b; Driscoll et al., 2007; Gur et al., 2006; Kim et al., 2003; Resnick et al., 2001, 2004, 2000, 2003; Stewart et al., 2006). It bears similarities with the "optimized VBM" approach (Good et al., 2002), except that it uses a highly conforming high-dimensional image warping algorithm that captures finer structural details. Moreover, it uses tissue-preserving transformations, which ensure that image warping preserves the absolute amounts of GM, WM, and CSF tissues present in an individual's scan, thereby allowing for precise local volumetric analysis.

PET images of resting-state rCBF were first co-registered with the MRI scans using mutual information, and then spatially normalized to the same template space based on the spatial normalization transformation parameters determined from the MRI. PET images were then intensity-normalized using proportional scaling, i.e. they were divided by the total counts in the brain.

Statistical analysis and pattern classification

The RAVENS maps and the spatially normalized PET images, all co-registered in the same template space, were smoothed by Gaussian filters of full-width at half-maximum (FWHM) smoothing kernels 6 mm and 15 mm, respectively. Group comparisons for MRI and PET images, separately, were performed via voxel-wise effect sizes.

Since the main goal of this paper is to test diagnostic tools for individual scans, rather than to identify statistical differences between two potentially overlapping groups, we applied high-dimensional pattern classification (Fan et al., 2007b) in addition to voxel-based group analyses. In particular, regional features were first extracted from brain regions/clusters exhibiting significant group differences examined by two-sample Hotelling's T-square statistic of tissue density and PET scan intensity values; local clusters were formed using a watershed-based region growing technique described in Fan et al. (2007b). A feature reduction process was then applied, using a feature selection method which identifies a minimal set of brain regions that jointly provide optimal separation between MCI and cognitively normal (CN) (Fan et al., 2007b). This step is very important, as it identifies a minimal set of regions, which will be referred to as optimally differentiating clusters (ODC) in the remainder of the paper, which jointly maximally differentiate between MCI and CN individuals on an individual scan basis. A linear support vector machine (SVM) classifier was finally trained based on features extracted from the ODC, which outputs a value, indicating a pattern resembling MCI when positive, or brain pattern in unimpaired individuals when negative. Local volumetric measurements, as defined by the values of the RAVENS maps, and rCBF were combined from all ODC into a measurement of spatial patterns of brain structure and physiology. Leave-one-out cross-validation was used to test this classification scheme on datasets not used for training. The pattern classification method provides a *structural–functional biomarker score* (*SFBS*). For a classifier constructed from the CN and MCI groups, positive *SFBS* implies MCI-like imaging profile, and vice-versa.

Evaluation via cross-validation and bagging

The procedure described earlier assumes that we know in advance the number of brain regions to use for building the classifier. Too few regions typically result in under-training, and too many regions cannot be supported by our limited sample size. In these experiments we report classification accuracy as a function of the number of regions that one can use. However, in practice, the number of brain regions is not known *a priori*. Therefore, and in order to evaluate the generalization performance of the high-dimensional pattern classification method under the assumption that it will automatically determine the best number of brain regions, the bagging-cross-validation technique was applied (Fan et al., 2008b). In particular, one subject is first selected as a test subject, and the remaining subjects are used for building an ensemble classifier whose parameters are automatically optimized in a bagging framework (Breiman, 1996). Bagging essentially applies a second cross-validation step within the training set, in order to determine the optimal parameters of the classifier. In particular, if n is the total number of subjects in the study, one is left out for testing, and the remaining $n-1$ are used for training. From these $n-1$ samples, we form $n-1$ different training sets, each time leaving one more subject out, thereby each time having a training set of $n-2$ subjects. For each of these training sets, the high-dimensional pattern classification method is used to build a classifier, referred to as a bootstrap classifier, whose performance is then evaluated on the $(n-1)th$ sample. This procedure is repeated $n-1$ times, once for each bootstrap classifier. This process allows us to determine the optimal parameters of the classifier, including the number of clusters that is used, so that the area under the ROC curve is maximized (Huang and Ling, 2005). The classifier is then tested on the *n-th* subject, the test subject, who has been completely left out of the entire training and parameter optimization process. It is important to note, here, that this process generates $n-1$ bootstrap classifiers. Therefore, when the test sample is to be classified, all $n-1$ classifiers are used, and their outputs s_i, $i=1,\ldots n-1$, are combined using voting, $v=2(\mathrm{card}\{s_i,>0|\ s_i,\ i=1,\ldots \mathrm{n}-1\}/(\mathrm{n}-1)-0.5)$. This provides the final classification score, i.e. the *SFBS*, which is compared with the true/known class of the test subject, in order to record classification errors. This process is repeated n times, each time leaving out a different subject, finally leading to an overall classification error obtained from n scans.

Results

MRI–PET-based subject classification accuracy

The classification rates obtained via leave-one-out cross-validation, as a function of the number of regions used in classification,

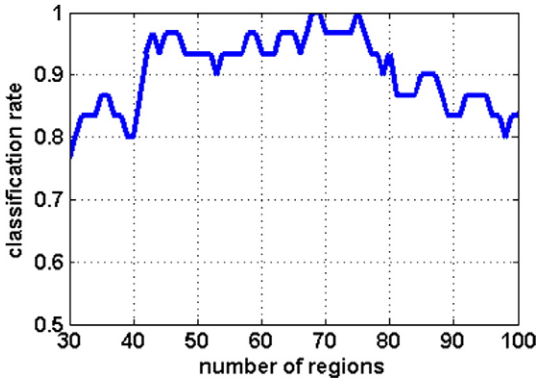

Fig. 1. The classification rate as a function of the number of regions used in classification.

are shown in the left column of Fig. 1. (Three values were used from each region: GM volume, WM volume, and average normalized PET signal; hence the total number of features was 3 times as many as the number of regions.) As Fig. 1 indicates, cross-validated classification performance can reach up to 100%. However, the classification accuracy tends to be around 93%, on the average, for a reasonable range of the number of brain regions used by the classifier (between 50 and 80 brain regions). In particular, Fig. 1 indicates that if we choose 68 or 75 brain regions, cross-validation estimates a 100% classification accuracy, as opposed to a maximum classification accuracy of 93% achieved via MRI only from the same participants (Davatzikos et al., 2008). Later in our experiments we also report the results obtained by letting the classifier choose the optimal number of brain regions, using the bagging approach, which provides a generally more conservative estimate of generalization accuracy of the classifier.

Spatial pattern of MCI specific abnormalities

As shown in Fig. 2, the high-dimensional pattern classification method identified optimally differentiating clusters of brain atrophy and reduced blood flow, which collectively contributed to the classification. As we discussed in the previous section, leave-one-out cross-validation was used to estimate the classification accuracy. In each repetition of this procedure, a different subject was left out, thereby resulting in a different set of $n-1$ bootstrap classifiers. Therefore, a total of $n*(n-1)$ classifiers was constructed, each of them possibly being slightly different from the other. In order to generate a visual picture of the brain regions that the collection of these classifiers evaluated for determination of the classification score, we calculated the number of bootstrap classifiers that used each region of the brain. This spatial map is shown in Fig. 2.

The conventional group analysis, via voxel-wise effect sizes separately on GM, WM, and PET, shows local maxima in regions of statistical significance (Fig. 3), which tend to be in agreement with the set of ODC depicted in Fig. 2. In general, these figures reveal that, in addition to the spatial pattern of atrophy, reduced

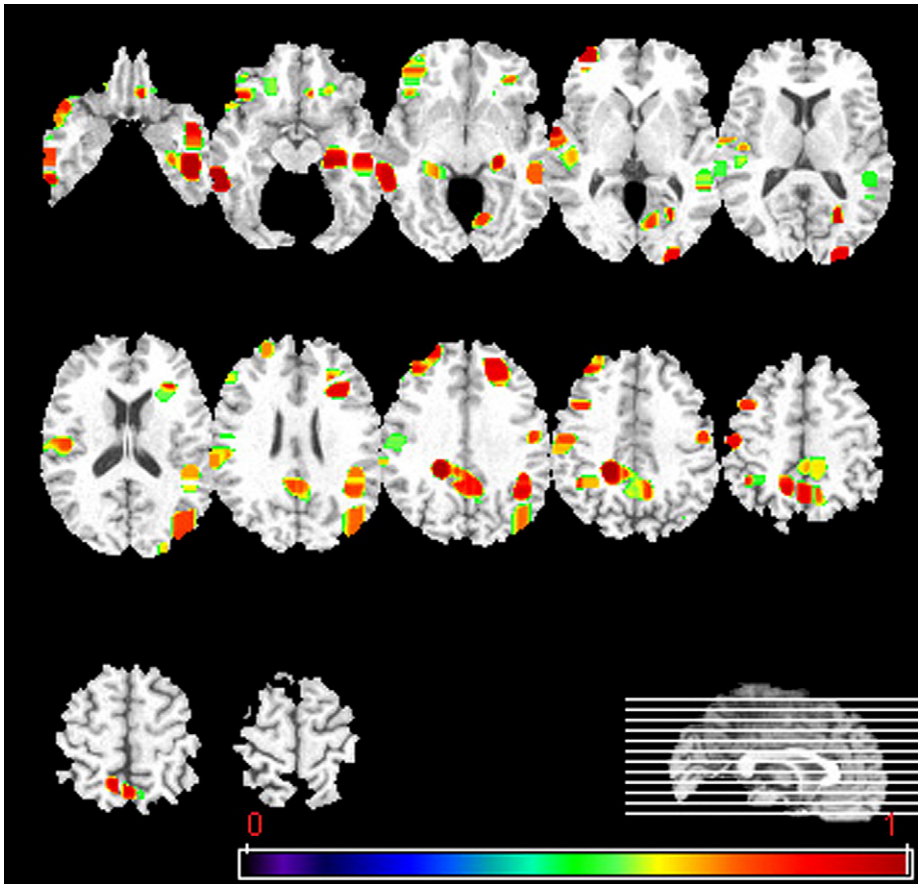

Fig. 2. Spatial patterns of structural and functional brain abnormality associated with MCI detected by the classification method. Brain regions that collectively contributed to the classification are overlaid on the template image. Images are displayed in radiological convention. The relatively most consistently used regions are shown in red or yellow.

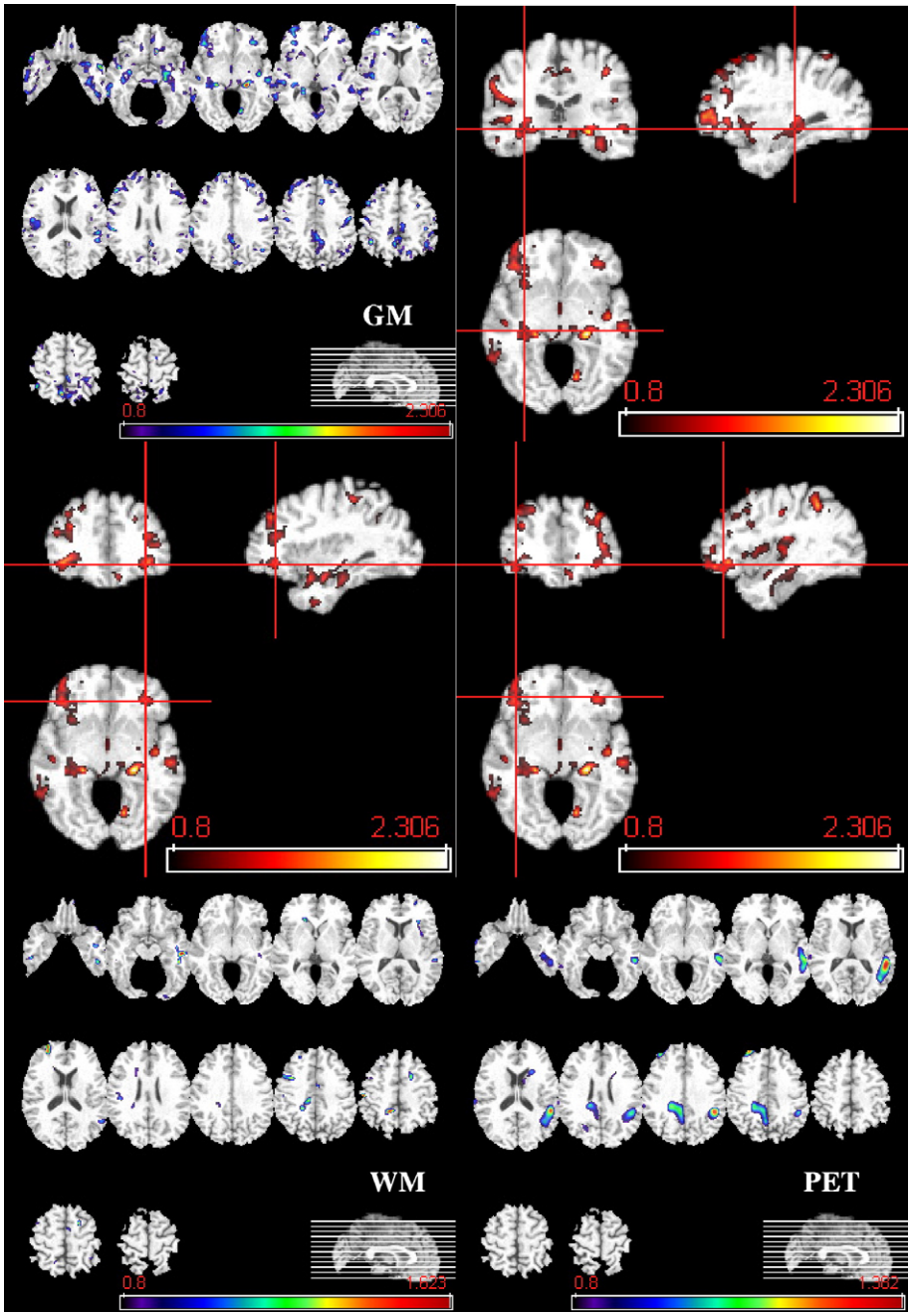

Fig. 3. Top left: Axial sections of effect size maps of group differences in GM. Top right and middle row: Tri-planar sections of effect size maps of group difference in GM. Bottom row: Axial sections of effect size maps of group differences in WM and PET. The color scales indicate CN > MCI. Images are in radiology convention.

blood flow in the right posterior cingulate and in the left language-related association cortex contributes to the best discrimination between the two groups.

Results from evaluation via cross-validation and bagging

As discussed earlier, Fig. 1 indicates that, if we knew that we should use 68 or 75 brain regions, we would achieve 100% classification accuracy, estimated via leave-one-out cross-validation. However, for different number of regions we would obtain somewhat lower performance. The procedure detailed in the Methods section entitled "Evaluation via cross-validation and bagging" does not rely on *a priori* knowledge of the number of regions, but instead it automatically determines that number as part of the bagging process. It, therefore, generally yields slightly lower classification accuracy estimates, but provides a better indicator of the generalization ability of the classifier on new studies. The performance of the ensemble classifiers discussed in that section is summarized in Fig. 4. The area under the ROC curve of the ensemble classifiers that aggregates the bootstrap classifiers equals to 0.978, which indicates excellent diagnostic value.

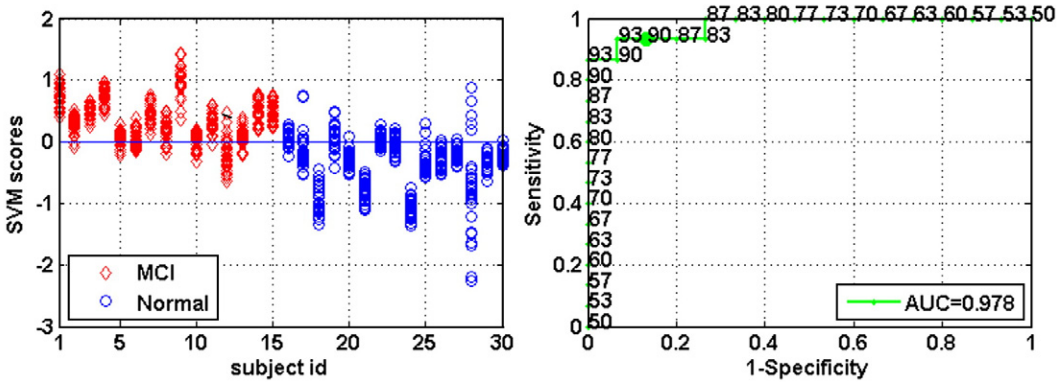

Fig. 4. Left: Distribution of SVM scores calculated via the leave-one-out bagging procedure described in the text. Right: ROC curve of the ensemble classifiers. Numbers around the curve are the correct classification rates (%) corresponding to different sensitivities and specificities. The bold face point on the curve corresponds to the classification rate with zero as the classification threshold.

When the bagging procedure was applied to the MRI data alone, without the joint evaluation with PET, an 87% accuracy was obtained (AUC=0.875). Using the PET images only, we obtained 50% classification accuracy.

Discussion

This study investigated the diagnostic value of imaging biomarkers, obtained by integrating structural and functional images via high-dimensional pattern classification, for discrimination of cognitively normal individuals from individuals with mild cognitive impairment. Complex spatial patterns of brain atrophy and blood flow were identified and found to have very high diagnostic accuracy that reached 100%, which is 6% higher than the maximum classification rate achieved from MRI only. A more conservative estimate of generalization performance, obtained via a procedure called bagging in conjunction with leave-one-out cross-validation, was 90%, with an area under the curve equal to 0.978, which was also about 3% higher than the respective accuracy obtained via MRI alone, and much higher than accuracy achieved via PET alone. These results indicate an excellent diagnostic value of the *SFBS*, especially in view of the relatively limited sample size available in this study.

A strength of our prospectively assessed cohort is that we were able to study MCI at a relatively mild stage of cognitive decline and presumably of underlying pathology. The early identification of MCI in our sample is an important distinction between the current study and other studies that involve patients reporting to the clinic with memory complaints.

Evaluation of the spatial patterns of brain atrophy indicated quite widespread, yet often subtle, reduction of mainly GM, but also WM volumes in a variety of brain regions, including the hippocampus, inferior temporal cortical GM and WM, insular and orbitofrontal GM, posterior cingulate, and precuneus. Two regions of reduced blood flow were also measured, namely the posterior cingulate and a fairly extended area in the left parietal and parieto-temporal cortex. Most of these regions are known to be affected by AD (Ardekani et al., 2007; Chetelat et al., 2002; Convit et al., 1997; Dickerson et al., 2001; Firbank et al., 2007; Fox and Schott, 2004; Fox et al., 1996b; Frisoni et al., 2007; Ishii et al., 2005a; Jack et al., 1999; Karas et al., 2007; Killiany et al., 2000; Krasuski et al., 1998; Matsuda et al., 2002; Pantano et al., 1999; Pennanen et al., 2005b; Thompson et al., 2007); however, it is their combination via high-dimensional pattern classification that leads to high diagnostic accuracy on an individual basis.

The pattern of reduced blood flow measured in our study was asymmetric, and in agreement with the findings of Minoshima et al. (1994b); Reiman et al. (1996b);and Scarmeas et al. (2004) who used PET ^{15}O imaging in an AD sample. A variety of PET studies in AD have demonstrated asymmetrically reduced blood flow or metabolic activity in AD patients (Foster et al., 1983; Ishii et al., 2005b; Kawachi et al., 2006; Koss et al., 1985; Martin et al., 1986) and in elderly individuals with cognitive decline (Hunt et al., 2007); however the biological underpinnings of these asymmetries are not quite known. Notably, these asymmetries are often reversed, implying that different individuals might be affected by, or compensate for, AD pathology differently. The pattern of reduced blood flow in association with MCI indicated decreases in posterior cingulate rCBF. Decreased neural activity in the posterior cingulate has been described in AD (e.g. Minoshima et al. (1994a) and in unaffected individuals who carry the Apolipoprotein E e4 risk factor for AD (Minoshima et al., 1994a; Reiman et al., 1996a).

Our findings suggest relatively symmetric brain atrophy, in contrast to some previous findings using VBM (Karas et al., 2004; Thompson et al., 2001). Although methodological differences in image analysis could also account for the differences of our findings and the ones in Karas et al. (2004), patient selection is also likely to be a factor. In particular, the study in Karas et al. (2004) was retrospective, whereas our study was prospective. Retrospective studies can be confounded by the fact that a relatively larger degree of right-hemisphere atrophy, compared to left, is likely to be tolerated before the patient reports to the clinic, since deficits in verbal memory are more likely to trigger a visit to the clinic relatively earlier. Prospective studies, however, tend to be more robust to such confounds. Moreover, our findings are consistent with histopathological studies of AD, which have found relatively symmetric patterns of brain atrophy (Braak et al., 1998).

The results of the high-dimensional pattern classification are very encouraging, since they indicate that sufficient sensitivity and specificity can be achieved for these tools to have diagnostic value in the clinic. Although 100% cross-validated classification accuracy was achieved for certain parameter settings, a more realistic estimate of the generalization accuracy of this approach is 90%, as the results of Fig. 4 indicated, which is based on automatic

estimation of a single number of brain clusters from the training set, instead of evaluating performance over a range of values for the number of clusters. This small discrepancy is mainly due to the small sample size available to us in this study, which typically leads to the jittery performance curves shown in Fig. 1 due to under-training of the classifier. Based on the curve of Fig. 1, we anticipate that more extensive training on larger sets of data will ultimately allow us to achieve stable classification performance close to 100%.

The set of ODC (Fig. 2) tended to be in agreement with the voxel-based analysis of the MRI and PET images (Fig. 3). However, the ODC approach yielded a more parsimonious number of brain clusters. This is to be expected, since the classification methodology inherently seeks the minimal number of brain clusters necessary for classification. Parsimonious models are of great value in interpreting the data, since they allow us to focus on the patterns of structural and functional changes that are most distinctive of MCI, thereby achieving a higher level of robustness. Interestingly, the spatial pattern of Fig. 2 fits with the known patterns of early AD pathology, spanning mainly the temporal lobe, the orbitofrontal cortex, and the posterior cingulate.

Although the majority of the neuroimaging literature of AD has focused on measuring regions that are most affected by the disease, such as the medial temporal lobe and posterior cingulate, our study suggests that patterns of structural and functional imaging characteristics must be evaluated to increase the accuracy of tools sufficient for diagnosis on an individual basis. These spatial patterns are complex and include many regions that are not known in advance. The methodology presented herein is built around this concept, namely that the set of brain measurements that optimally differentiates between the two groups cannot be known *a priori*, but is determined from the data. However, since leave-one-out cross-validation was used, the optimal set of clusters was always tested on new, previously unseen scans. This is fundamentally important, and guards against over-fitting the data, a problem analogous to that of multiple comparisons in VBM analyses.

Important for achieving high classification rate was not only the combination of many brain regions, but also the combination of PET and MRI. MRI alone had far superior classification accuracy than PET when each modality was used alone. However, the combination of the two provided the best results, suggesting that PET offers additional and somewhat complementary information to MRI. The combination of the two modalities is important for an additional reason, namely that changes in blood flow can be attributed, in part, to brain atrophy. Although regional measurements of brain atrophy could be used to normalize the PET signal, the fully multivariate approach followed herein offers a more general and comprehensive way of examining the data.

While the current study aims to develop an imaging-based diagnostic tool, it only takes one step in that direction. Our study examines the ability to distinguish between amnestic MCI and cognitively normal groups but does not include all possible types of dementia. For example, we do not test the ability of this classifier to distinguish between early stages of frontotemporal dementia and early stages of AD. However, this type of multi-class classification problem is generally a relatively straightforward extension of the two-group problem (Duda et al., 2001). In particular, multi-class classification is often achieved by applying a number of pair-wise two-class classifiers, and then combining the results using voting. Multi-class support vector machine classifiers are also available.

In summary, this study combined structural MRI and blood flow PET images in a high-dimensional pattern classification framework, which achieved up to 100% accuracy in classifying individual scans of patients with relatively mild MCI in a prospective longitudinal study of aging. The results indicate that high-dimensional classification, partly built upon voxel-based multivariate analysis of the integration of structural and functional images, has the potential to serve as an early diagnostic tool for AD on an individual patient basis. Future studies on larger samples, as well as on healthy elderly individuals with cognitive decline, will further test whether these structural and physiological alterations seen in this MCI cohort are replicated robustly and perhaps at even earlier disease stages. These diagnostic tests have a great potential in complementing standard neurological examinations, especially in evaluating disease progression reliably and quantitatively.

Acknowledgments

This study was supported in part by NIH funding sources N01-AG-3-2124 and R01-AG14971 and by the Intramural Research Program of the NIH, National Institute on Aging.

References

Ardekani, S., Kumar, A., Bartzokis, G., Sinha, U., 2007. Exploratory voxel-based analysis of diffusion indices and hemispheric asymmetry in normal aging. Magn. Res. Imaging 25, 154–167.

Ashburner, J., Friston, K.J., 2000. Voxel-based morphometry: the methods. Neuroimage 11, 805–821.

Ashburner, J., Csernansky, J.G., Davatzikos, C., Fox, N.C., Frisoni, G.B., Thompson, P.M., 2003. Computer-assisted imaging to assess brain structure in healthy and diseased brains. Lancet (Neurology) 2, 79–88.

Beresford, T., Arciniegas, D., Alfers, J., Clapp, L., Martin, B., Beresford, H., Du, Y., Liu, D., Shen, D., Davatzikos, C., Laudenslager, M., 2006a. Hypercortisolism in alcohol dependence and its relation to hippocampal volume loss. J. Stud. Alcohol 67, 861–867.

Beresford, T.P., Arciniegas, D.B., Alfers, J., Clapp, L., Martin, B., Du, Y., Liu, D., Shen, D., Davatzikos, C., 2006b. Hippocampus volume loss due to chronic heavy drinking. Alcohol., Clin. Exp. Res. 30, 1866–1870.

Bozzali, M., Filippi, M., Magnani, G., Cercignani, M., Franceschi, M., Schiatti, E., Castiglioni, S., Mossini, R., Falautano, M., Scotti, G., Comi, G., Falini, A., 2006. The contribution of voxel-based morphometry in staging patients with mild cognitive impairment. Neurology 67, 453–460.

Braak, H., Braak, E., Bohl, J., Bratzke, H., 1998. Evolution of Alzheimer's disease related cortical lesions. J. Neural Transm., Suppl. 54, 97–106.

Breiman, L., 1996. Bagging predictors. Mach. Learn. 24, 123–140.

Chetelat, G., Desgranges, B., de la Sayette, V., Viader, F., Eustache, F., Baron, J.-C., 2002. Mapping gray matter loss with voxel-based morphometry in mild cognitive impairment. Neuroreport 13, 1939–1943.

Chung, M.K., Worsley, K.J., Paus, T., Cherif, C., Collins, D.L., Giedd, J.N., Rapoport, J.L., Evans, A.C., 2001. A unified statistical approach to deformation-based morphometry. Neuroimage 14, 595–606.

Convit, A., De Leon, M.J., Tarshish, C., De Santi, S., Tsui, W., Rusinek, H., George, A., 1997. Specific hippocampal volume reductions in individuals at risk for Alzheimer's disease. Neurobiol. Aging 18, 131–138.

Convit, A., de Asis, J., de Leon, M.J., Tarshish, C.Y., De Santi, S., Rusinek, H., 2000. Atrophy of the medial occipitotemporal, inferior, and middle temporal gyri in non-demented elderly predict decline to Alzheimer's disease. Neurobiol. Aging 21, 19–26.

Davatzikos, C., 2004. Why voxel-based morphometric analysis should be used with great caution when characterizing group differences. NeuroImage 23, 17–20.

Davatzikos, C., Vaillant, M., Resnick, S., Prince, J.L., Letovsky, S., Bryan, R.N., 1996. A computerized approach for morphological analysis of the corpus callosum. J. Comput. Assist. Tomogr. 20, 88–97.

Davatzikos, C., Genc, A., Xu, D., Resnick, S.M., 2001. Voxel-based morphometry using the RAVENS maps: methods and validation using simulated longitudinal atrophy. NeuroImage 14, 1361–1369.

Davatzikos, C., Ruparel, K., Fan, Y., Shen, D., Acharyya, M., Loughead, J., Gur, R.C., Langleben, D., 2005a. Classifying spatial patterns of brain activity for lie-detection. Neuroimage 28, 663–668.

Davatzikos, C., Shen, D.G., Wu, X., Lao, Z., Hughett, P., Turetsky, B.I., Gur, R.C., Gur, R.E., 2005b. Whole-brain morphometric study of schizophrenia reveals a spatially complex set of focal abnormalities. JAMA Arch. Gen. Psychiatry 62, 1218–1227.

Davatzikos, C., Fan, Y., Wu, X., Shen, D., Resnick, S.M., 2008. Detection of prodromal Alzheimer's Disease via pattern classification of MRI. Neurobiology of Aging 29, 514–523.

Dickerson, B.C., Goncharova, I., Sullivan, M.P., Forchetti, C., Wilson, R.S., Bennett, D.A., Beckett, L.A., deToledo-Morrell, L., 2001. MRI-derived entorhinal and hippocampal atrophy in incipient and very mild Alzheimer's disease. Neurobiol. Aging 22, 747–754.

Driscoll, I., Davatzikos, C., An, Y., Wu, X., Shen, D., Kraut, M., Resnick, S.M., 2007. Longitudinal Brain Changes in Cognitively Impaired and Unimpaired Older Adults. Society of neuroscience, San Diego, CA.

Duchesne, S., Bernasconi, N., Bernasconi, A., Collins, D.L., 2006. MR-based neurological disease classification methodology: application to lateralization of seizure focus in temporal lobe epilepsy. Neuroimage 29, 557–566.

Duda, R.O., Hart, P.E., Stork, D.G., 2001. Pattern Classification. John Wiley and Sons, Inc.

Fan, Y., Shen, D., Davatzikos, C., 2005. Classification of structural images via high-dimensional image warping, robust feature extraction, and SVM. In: Duncan, J.S., Gerig, G. (Eds.), MICCAI. Springer, Berlin/Heidelberg, pp. 1–8. Palm Springs, California, USA.

Fan, Y., Rao, H., Giannetta, J., Hurt, H., Wang, J., Davatzikos, C., Shen, D., 2006a. Diagnosis of Brain Abnormality Using both Structural and Functional MR Images. IEEE EMBS, New York City, NY, USA, pp. 1044–1047.

Fan, Y., Shen, D., Davatzikos, C., 2006b. Decoding cognitive states from fMRI images of subjects by machine learning and multivariate classification. IEEE Workshop on Mathematical Methods in Biomedical Image (MMBIA 2006). New York City, NY, USA.

Fan, Y., Rao, H., Hurt, H., Giannetta, J., Korczykowski, M., Shera, D., Avants, B.B., Gee, J.C., Wang, J., Shen, D., 2007a. Multivariate examination of brain abnormality using both structural and functional MRI. Neuroimage 36, 1189–1199.

Fan, Y., Shen, D., Gur, R.C., Gur, R.E., Davatzikos, C., 2007b. COMPARE: Classification of Morphological Patterns using Adaptive Regional Elements. IEEE Trans. Med. Imag. 26, 93–105.

Fan, Y., Gur, R.E., Gur, R.C., Wu, X., Shen, D., Calkins, M.E., Davatzikos, C., 2008a. Unaffected family members and schizophrenia patients share brain structure patterns: a high-dimensional pattern classification study. Biol. Psychiatry 63, 118–124.

Fan, Y., Resnick, S.M., Davatzikos, C., 2008b. Feature Selection and Classification of Multi-Parametric Medical Images Using Bagging and SVM. SPIE medical Imaging, San Diego, California, USA.

Firbank, M.J., Blamire, A.M., Krishnan, M.S., Teodorczuk, A., English, P., Gholkar, A., Harrison, R., O'Brien, J.T., 2007. Atrophy is associated with posterior cingulate white matter disruption in dementia with Lewy bodies and Alzheimer's disease. NeuroImage 36, 1–7.

Foster, N.L., Chase, T.N., Fedio, P., Patronas, N.J., Brooks, R.A., Chiro, G.D., 1983. Alzheimer's disease: focal cortical changes shown by positron emission tomography. Neurology 33, 961–965.

Fox, N., Schott, J., 2004. Imaging cerebral atrophy: normal ageing to Alzheimer's disease. Lancet 363, 392–394.

Fox, N., Warrington, E., Freeborough, P., Hartikainen, P., Kennedy, A., Stevens, J., Rossor, M., 1996a. Presymptomatic hippocampal atrophy in Alzheimer's disease. A longitudinal MRI study. Brain 119, 2001–2007.

Fox, N.C., Freeborough, P.A., Rossor, M.N., 1996b. Visualisation and quantification of rates of atrophy in Alzheimer's disease. Lancet 348, 94–97.

Frisoni, G.B., Pievani, M., Testa, C., Sabattoli, F., Bresciani, L., Bonetti, M., Beltramello, A., Hayashi, K.M., Toga, A.W., Thompson, P.M., 2007. The topography of grey matter involvement in early and late onset Alzheimer's disease. Brain 130, 720–730.

Goldszal, A.F., Davatzikos, C., Pham, D., Yan, M., Bryan, R.N., Resnick, S.M., 1998. An image processing protocol for the analysis of MR images from an elderly population. J. Comput. Ass. Tomogr. 22, 827–837.

Golland, P., Fischl, B., Spiridon, M., Kanwisher, N., Buckner, R.L., Shenton, M.E., Kikinis, R., Dale, A., Grimson, W.E.L., 2002. Discriminative analysis for image-based studies. In: Dohi, T., R.K. (Eds.), Fifth International Conference on Medical Image Computing and Computer Assisted Intervention. Springer-Verlag GmbH, Tokyo, Japan, pp. 508–515.

Good, C.D., Scahill, R.I., Fox, N.C., Ashburner, J., Friston, K.J., Chan, D., Crum, W.R., Rossor, M.N., Frackowiak, R.S.J., 2002. Automatic differentiation of anatomical patterns in the human brain: Validation with studies of degenerative dementias. Neuroimage 17, 29–46.

Grundman, M., et al., 2004. Mild cognitive impairment can be distinguished from Alzheimer disease and normal aging for clinical trials. Arch. Neurol. 61, 59–66.

Gur, R., Davatzikos, C., Shen, D., Wu, X., Fan, Y., Hughett, P., Turetsky, B., Gur, R., 2006. Whole-brain deformation based morphometry MRI study of schizophrenia. Schizophr. Bull. 31, 408–408.

Huang, J., Ling, C.X., 2005. Using AUC and accuracy in evaluating learning algorithms. IEEE Trans. Knowl. Data Eng. 17, 299–310.

Hunt, A., Schönknecht, P., Henze, M., Seidl, U., Haberkorn, U., Schröder, J., 2007. Reduced cerebral glucose metabolism in patients at risk for Alzheimer's disease. Psychiatry Res. 155, 147–154.

Ishii, K., Kawachi, T., Sasaki, H., Kono, A., Fukuda, T., Kojima, Y., Mori, E., 2005a. Voxel-based morphometric comparison between early- and late-onset mild Alzheimer's disease and assessment of diagnostic performance of z score images. AJNR Am. J. Neuroradiol. 26, 333–340.

Ishii, K., Sasaki, H., Kono, A.K., Miyamoto, N., Fukuda, T., Mori, E., 2005b. Comparison of gray matter and metabolic reduction in mild Alzheimer's disease using FDG-PET and voxel-based morphometric MR studies. Eur. J. Nucl. Med. Mol. Imag. 32, 959–963.

Jack, C.R., Petersen, R.C.,Y.C.,X., O'Brien, P.C., Smith, G.E., Ivnik, R.J., Boeve, B.F., Waring, S.C., Tangalos, E., Kokmen, E., 1999. Prediction of AD with MRI-based hippocampal volume in mild cognitive impairment. Neurology 52, 1397–1403.

Kabani, N., MacDonald, D., Holmes, C.J., Evans, A., 1998. A 3D atlas of the human brain. Neuroimage 7, S717.

Karas, G.B., Scheltens, P., Rombouts, S.A.R.B., Visser, P.J., Schijndel, R.A.v., Fox, N.C., Barkhof, F., 2004. Global and local gray matter loss in mild cognitive impairment and Alzheimer's disease. Neuroimage 23, 708–716.

Karas, G., Scheltens, P., Rombouts, S., van Schijndel, R., Klein, M., Jones, B., van der Flier, W., Vrenken, H., Barkhof, F., 2007. Precuneus atrophy in early-onset Alzheimer's disease: a morphometric structural MRI study. Neuroradiology 49, 967–976.

Kawachi, T., Ishii, K., Sakamoto, S., Sasaki, M., Mori, T., Yamashita, F., Matsuda, H., Mori, E., 2006. Comparison of the diagnostic performance of FDG-PET and VBM-MRI in very mild Alzheimer's disease. Eur. J. Nucl. Med. Mol. Imag. 33, 801–809.

Kawasaki, Y., Suzuki, M., Kherif, F., Takahashi, T., Zhou, S.-Y., Nakamura, K., Matsui, M., Sumiyoshi, T., Seto, H., Kurachi, M., 2007. Multivariate voxel-based morphometry successfully differentiates schizophrenia patients from healthy controls. Neuroimage 34, 235–242.

Kaye, J., Swihart, T., Howieson, D., Dame, A., Moore, M., Karnos, T., Camicioli, R., Ball, M., Oken, B., Sexton, G., 1997. Volume loss of the hippocampus and temporal lobe in healthy elderly persons destined to develop dementia. Neurology 48, 1297–1304.

Killiany, R.J., Gomez-Isla, T., Moss, M., Kikinis, R., Sandor, T., Jolesz, F., Tanzi, R., Jones, K., Hyman, B.T., Albert, M.S., 2000. Use of structural magnetic resonance imaging to predict who will get Alzheimer's disease Temporal lobe regions on magnetic resonance imaging identify patients with early Alzheimer's disease. Ann. Neurol. 47, 430–439.

Kim, J.-S., Kanaan, R., Kaufmann, W., Ross, C., Calhoun, V., Xu, D., Shen, D., Davatzikos, C., Godfrey Pearlson, G.D., 2003. Abnormal White

Matter Organization in Huntington's Disease Evaluated with Diffusion Tensor MRI. ISMRM, Toronto, Canada.

Koss, E., Friedland, R.P., Ober, B.A., Jagust, W.J., 1985. Differences in lateral hemispheric asymmetries of glucose utilization between early- and late-onset Alzheimer-type dementia. Am. J. Psychiatry 142, 638–640.

Krasuski, J.S., Alexander, G.E., Horwitz, B., Daly, E.M., Murphy, D.G., Rapoport, S.I., Schapiro, M.B., 1998. Volumes of medial temporal lobe structures in patients with Alzheimer's disease and mild cognitive impairment (and in healthy controls). Biol. Psychiatry 43, 60–68.

Lao, Z., Shen, D., Xue, Z., Karacali, B., Resnick, S.M., Davatzikos, C., 2004. Morphological classification of brains via high-dimensional shape transformations and machine learning methods. Neuroimage 21, 46–57.

Liu, Y., Teverovskiy, L., Carmichael, O., Kikinis, R., Shenton, M., Carter, C.S., Stenger, V.A., Davis, S., Aizenstein, H., Becker, J., Lopez, O., Meltzer, C., 2004. Discriminative MR image feature analysis for automatic schizophrenia and Alzheimer's disease classification. In: Barillot, C., Haynor, R., David, Hellier, Pierre (Eds.), Medical Image Computing and Computer-Assisted Intervention — MICCAI 2004: 7th International Conference. Springer-Verlag GmbH, Saint-Malo, France, pp. 393–401.

Martin, A., Brouwers, P., Lalonde, F., Cox, C., Teleska, P., Fedio, P., Foster, N., Chase, T., 1986. Towards a behavioral typology of Alzheimer's patients. J. Clin. Exp. Neuropsychol. 8, 594–610.

Matsuda, H., Kitayama, N., Ohnishi, T., Asada, T., Nakano, S., Sakamoto, S., Imabayashi, E., Katoh, A., 2002. Longitudinal evaluation of both morphologic and functional changes in the same individuals with Alzheimer's disease. J. Nucl. Med. 43, 304–311.

Miller, M., Banerjee, A., Christensen, G., Joshi, S., Khaneja, N., Grenander, U., Matejic, L., 1997. Statistical methods in computational anatomy. Stat. Methods Med. Res. 6, 267–299.

Minoshima, S., Foster, N., Kuhl, D., 1994a. Posterior cingulate cortex in Alzheimer's disease. Lancet 344, 895.

Minoshima, S., Foster, N.L., Kuhl, D.E., 1994b. Posterior cingulate cortex in Alzheimer's disease. Lancet 344, 895.

Morris, J.C., Heyman, A., Mohs, R.C., Hughes, J.P., van Belle, G., Fillenbaum, G., Mellits, E.D., Clark, C., 1989. The Consortium to Establish a Registry for Alzheimer's Disease (CERAD). Part I. Clinical and neuropsychological assessment of Alzheimer's disease. Neurology 39, 1159–1165.

Mourao-Miranda, J., Bokde, A.L.W., Born, C., Hampel, H., Stetter, M., 2005. Classifying brain states and determining the discriminating activation patterns: support vector machine on functional MRI data. Neuroimage 28, 980–995.

Pantano, P., Caramia, F., Pierallini, A., 1999. The role of MRI in dementia. Ital. J. neurol. Sci. 20, S250–S253.

Pennanen, C., Testa, C., Laakso, M.P., Hallikainen, M., Helkala, E.-L., Hänninen, T., Kivipelto, M., Könönen, M., Nissinen, A., Tervo, S., Vanhanen, M., Vanninen, R., Frisoni, G.B., Soininen, H., 2005a. A voxel based morphometry study on mild cognitive impairment. J. Neurol. Neurosurg. Psychiatry 76, 11–14.

Pennanen, C., Testa, C., Laakso, M.P., Hallikainen, M., Helkala, E.L., Hanninen, T., Kivipelto, M., Kononen, M., Nissinen, A., Tervo, S., Vanhanen, M., Vanninen, R., Frisoni, G.B., Soininen, H., 2005b. A voxel based morphometry study on mild cognitive impairment. J. Neurol. Neurosurg. Psychiatry 76, 11–14.

Petersen, R.C., Smith, G.E., Waring, S.C., Ivnik, R.J., Tangalos, E.G., Kokmen, E., 1999. Mild cognitive impairment: clinical characterization and outcome. Arch. Neurol. 56, 303–308.

Pham, D.L., Prince, J.L., 1999. Adaptive fuzzy segmentation of magnetic resonance images. IEEE Trans. Med. Imag. 18, 737–752.

Reiman, E., Caselli, R., Yun, L., Chen, K., Bandy, D., Minoshima, S., Thibodeau, S., Osborne, D., 1996a. Preclinical evidence of Alzheimer's disease in persons homozygous for the epsilon 4 allele for apolipoprotein E. N. Engl. J. Med. 334, 752–758.

Reiman, E.M., Caselli, R.J., Yun, L.S., Chen, K., Bandy, D., Minoshima, S., Thibodeau, S.N., Osborne, D., 1996b. Preclinical evidence of Alzheimer's disease in persons homozygous for the epsilon 4 allele for apolipoprotein E. N. Engl. J. Med. 334, 752–758.

Resnick, S.M., Goldszal, A., Davatzikos, C., Golski, S., Kraut, M.A., Metter, E.J., Bryan, R.N., Zonderman, A.B., 2000. One-year age changes in MRI brain volumes in older adults. Cereb. Cortex 10, 464–472.

Resnick, S., Davatzikos, C., Kraut, M., Zonderman, A., 2001. Longitudinal changes in MRI volumes in older adults. Neurobiol. Aging 22, 5.

Resnick, S.M., Pham, D.L., Kraut, M.A., Zonderman, A.B., Davatzikos, C., 2003. Longitudinal Magnetic Resonance Imaging studies of older adults: a shrinking brain. J. Neurosci. 23, 295–301.

Resnick, S., Pham, D., Davatzikos, C., Kraut, M., 2004. Sex differences in regional cerebral blood flow: clinical implications for Alzheimer's disease. Neurobiol. Aging 25 (263), 2004.

Saykin, A.J., Wishart, H.A., Rabin, L.A., Santulli, R.B., Flashman, L.A., West, J.D., McHugh, T.L., Mamourian, A.C., 2006. Older adults with cognitive complaints show brain atrophy similar to that of amnestic MCI. Neurology 67, 834–842.

Scarmeas, N., Habeck, C.G., Zarahn, E., Anderson, K.E., Park, A., Hilton, J., Pelton, G.H., Tabert, M.H., Honig, L.S., Moeller, J.R., Devanand, D.P., Stern, Y., 2004. Covariance PET patterns in early Alzheimer's disease and subjects with cognitive impairment but no dementia: utility in group discrimination and correlations with functional performance. Neuroimage 23, 35–45.

Shen, D., Davatzikos, C., 2002. HAMMER: Hierarchical attribute matching mechanism for elastic registration. IEEE Trans. Med. Imag. 21, 1421–1439.

Shen, D.G., Davatzikos, C., 2003. Very high resolution morphometry using mass-preserving deformations and HAMMER elastic registration. NeuroImage 18, 28–41.

Stewart, W.F., Schwartz, B.S., Davatzikos, C., Shen, D., Liu, D., Wu, X., Todd, A.C., Shi, W., Bassett, S., Youssem, D., 2006. Past adult lead exposure is linked to neurodegeneration measured by brain MRI. Neurology 66, 1476–1484.

Thompson, P.M., Mega, M.S., Woods, R.P., Zoumalan, C.I., Lindshield, C.J., Blanton, R.E., Moussai, J., Holmes, C.J., Cummings, J.L., Toga, A.W., 2001. Cortical change in Alzheimer's disease detected with a disease-specific population-based brain atlas. Cereb. Cortex 11, 1–16.

Thompson, P., Hayashi, K., Dutton, R., Chiang, M., Leow, A., Sowell, E., De Zubicaray, G., Becker, J., Lopez, O., Aizenstein, H., Toga, A., 2007. Tracking Alzheimer's disease. Ann. N. Y. Acad. Sci. 1097, 183–214.

Timoner, S.J., Golland, P., Kikinis, R., Shenton, M.E., Grimson, W.E.L., Wells, W.M., 2002. Performance Issues in Shape Classification. Proceedings of the Fifth International Conference on Medical Image Computing and Computer-Assisted Intervention — MICCAI'02. Springer-Verlag, Tokyo, Japan, pp. 355–362.

Whitwell, J.L., Przybelski, S.A., Weigand, S.D., Knopman, D.S., Boeve, B.F., Petersen, R.C., Jack, C.R., 2007. 3D maps from multiple MRI illustrate changing atrophy patterns as subjects progress from mild cognitive impairment to Alzheimer's disease. Brain 130, 1777–1786.

Xie, S., Xiao, J.X., Gong, G.L., Zang, Y.F., Wang, Y.H., Wu, H.K., Jiang, X.X., 2006. Voxel-based detection of white matter abnormalities in mild Alzheimer disease. Neurology 66, 1845–1849.

Yoon, U., Lee, J.-M., Im, K., Shin, Y.-W., Cho, B.H., Kim, I.Y., Kwon, J.S., Kim, S.I., 2007. Pattern classification using principal components of cortical thickness and its discriminative pattern in schizophrenia. Neuroimage 34, 1405–1415.